HHS Public Access

Author manuscript

J Phys Chem B. Author manuscript; available in PMC 2019 March 13.

Published in final edited form as:

J Phys Chem B. 2016 April 14; 120(14): 3551–3559. doi:10.1021/acs.jpcb.5b12299.

Temperature-dependent Conformational Properties of Human Neuronal Calcium Sensor-1 Protein Revealed by All-atom Simulations

Yuzhen Zhu[1], **Buyong Ma**[2], **Ruth Nussinov**[2,3], and **Qingwen Zhang**[1,*]

[1]College of Physical Education and Training, Shanghai University of Sport, 399 Chang Hai Road, Shanghai, 200438, China

[2]Basic Science Program, Leidos Biomedical Research, Inc. Cancer and Inflammation Program, National Cancer Institute, Frederick, Maryland 21702, United States

[3]Sackler Inst. of Molecular Medicine Department of Human Genetics and Molecular Medicine Sackler School of Medicine, Tel Aviv University, Tel Aviv 69978, Israel

Abstract

Neuronal calcium sensor-1 (NCS-1) protein has orthologues from Saccharomyces cerevisiae (Frq1) to human with highly conserved amino acid sequences. NCS-1 is an important factor controlling the animal's response to temperature change. This leads us to investigate the temperature effects on the conformational dynamics of the human NCS-1 at 310 K and 316 K by extensive all-atom explicit-solvent molecular dynamics (MD) simulations and dynamic community network analysis. Four independent 500-ns MD simulations shows that the secondary structure content at 316 K is similar to that at 310 K, whereas the global protein structure is expanded at the elevated temperature. The elevated temperature results in loop 3 (L3) adopting an extended state that occupies the hydrophobic crevice, thereby blocking the binding of NCS-1 protein to its receptors. The number of suboptimal communication paths starting at residue D176 and ending at V190 in the L3 C-terminal tail is reduced with the elevation of temperature. The dynamic community network analysis suggests that the correlation between the N- and C-domain is weakened and the intradomain coupling is strengthened at 316 K. The elevation of temperature reduces the number of the salt bridges, especially in the C-domain, which may induce the conformational dynamic changes. This study suggests that the elevated temperature affects the conformational dynamics of human NCS-1 protein. Comparison of the structural dynamics of R102Q mutant and Δ176–190 truncated NCS-1 suggests that the structural and dynamics response of NCS-1 protein to elevation of temperature may be one of its intrinsic functional properties.

[*]**Corresponding Author:** zqw@sus.edu.cn.

Supporting Information

Seven figures present time evolution of average distances between three Ca^{2+} ions and amino acid residues coordinating to the Ca^{2+} for NCS-1 protein at 310 K during the 0~500 ns scales, time evolution of the number of backbone H-bonds and the helix percentage, the secondary structure profiles, distribution of the H-bonds number, the Cα-RMSF of each residue, cartoon representative structures of NCS-1 protein from the MD trajectories at 500 ns, time evolution of the radius of gyration at two different temperatures.

The authors declare no competing financial interest.

Keywords

Human neuronal calcium sensor 1 (NCS-1) protein; conformational dynamics; suboptimal communication paths; dynamic community network analysis; salt bridge; molecular dynamics simulations

1. INTRODUCTION

Human body temperature is tightly controlled at approximately 37°C. Fever is common in critically ill patients, including those with acute neurologic or neurosurgical disorders.[1–2] On the other hand, deliberate hyperthermia, as high as 43°C, has been used clinically as experimental therapy for neoplastic and infectious disease.[3] However, at elevated temperature, such as >40°C–41°C, there is increasing risk of brain damage and the initiation or worsening of multisystem failure.[1, 3] While the molecular mechanism of the temperature effect on human is not entirely understood, the thermotransduction cascades in *C. elegans* are much better studied.[4] Certain thermoreceptor neurons are sensitive to tiny thermal fluctuations (0.01°C or less) and maintain their sensitivity across a wide range of ambient temperatures through a process of adaptation, and receptor guanylate cyclases (GCY-8), phosphodiesterase (PDE-2), and neuronal calcium sensor (NCS-1) are critical elements in the AFD neurons responsible for *C. elegans* thermotaxis.[5] On a radial temperature gradient, *C. elegans* migrate toward their cultivation temperature and move along this isotherm, and this learning and memory are regulated by Ca^{2+} signaling via NCS-1.[6–7]

The neuronal calcium sensor (NCS) family is mostly expressed in neurons and currently includes 15 members,[8–9] among which NCS-1, recoverin and GCAP1 have similar main chain topologies.[10] The amino acid sequences of the NCS protein are conserved from yeast to humans and their sequence identities range from 35% to 60%.[10] They are distinguished by having a high affinity for Ca^{2+} and certain family members are palmitoylated (certain KChIPs) or N-terminal myristoylated, such as NCS-1, VILIPs, recoverin and KChIP1.[11] Some NCS proteins display reversible membrane association through a unique Ca^{2+}/myristoyl switch mechanism.[12–13] However, despite having high levels of sequence identity and structural similarity the NCS proteins have a number of known non-redundant functions.[14–15]

Neuronal calcium sensor-1 (NCS-1) protein is the most ancient member of the NCS family,[16] which has orthologues from Saccharomyces cerevisiae (Frq1)[17] to man. NCS-1 is N-terminally myristoylated allowing its association with distinct membrane compartments including the plasma membrane and the trans-Golgi network,[12] and it cycles between membrane-bound and cytosolic pools.[18] At the organism level, studies identified several key physiological functions for NCS-1 taking place through different pathways.[15] NCS-1 interacts with another Ca^{2+} sensor PICK1 that mediates long-term depression (LTD) in rat cortical neurons.[19] In the mouse, NCS-1 is implicated in the exploratory behavior and in the acquisition of spatial memory by regulating the surface expression of dopamine D2 receptors in the hippocampal dentate gyrus.[20] A study in Drosophila showed that NCS-1 regulates nerve terminal growth[21] through an interaction with the voltage-gated Ca^{2+} channel cacophony.[22]

Human NCS-1 plays critical roles in central neuronal system disorders and is associated with psychiatric diseases.[23] A rare missense mutation, substituting R102Q was identified in an autistic patient.[24] Previous studies[18, 25–26] have already demonstrated that the R102Q mutation produced pronounced distant as well as local changes, particularly in helices H6, H9 and loop L3. The dysfunctions of NCS-1 are poorly characterized on the molecular level.[16] A molecular dynamics (MD) simulation study showed that the R102Q mutation could affect the mobility of helix H9 and loop L3, compromising the docking of L3 into the hydrophobic crevice (HC).[25] Our recent MD simulation study showed that the C-terminal tail of loop L3 adopts a more extended state in the R102Q mutant, largely occupying the HC.[27] In a complex, HC is occupied by a Pik1 peptide fragment[28–30] and polyethylene glycol (PEG) molecules[31] which stabilize the conformation.[26] In the absence of ligand, L3 binds directly to the HC pocket as a ligand mimetic and regulates the conformational stability of the activated state.[26] A MD simulation study has shown that loop L3 docked into the HC during the first 20 ns, gaining a placement similar to that in the NMR structure.[25]

Recently key structural elements in the regulation of the temperature-dependent locomotion in *C. elegans* were characterized, pointing to the exposed hydrophobic groove and the role of the non-conserved C-terminal tail.[11] The amino acid sequences identities between *C. elegans* and human NCS-1 protein is 75.4%, and it is unclear whether the temperature change can affect the structure of the human NCS-1 protein. In this study, we examined loop L3 and the HC pocket of the human NCS-1 protein in the normal and the upper limit of human body temperature. We conducted two independent 500-ns MD simulations with explicit solvent for wild type NCS-1 at 310 K and 316 K, starting from two different initial structures. We found that the elevated temperature facilitates a more extended state of loop L3 within HC and reduction of the connectivity between D176 and V190 in the L3 C-terminal tail. Our dynamic community network analysis of the MD simulation trajectories illustrates that the elevated temperature weakens the interdomain correlation. The salt bridge network is altered, especially dramatically reducing the number and probability of salt bridges in the C-domain, which may be the reason for the conformational dynamic changes. Detailed analysis reveals that the human NCS-1 protein is sensitive to the solvent temperature and the computational results are consistent with our hypothesis. This study may provide atomic structural insights into temperature effects on key structural elements of human NCS-1 protein.

2. MATERIALS AND METHODS

Human NCS-1 protein.

The first two minimum energy models of 20 solution NMR structures (PDB entry 2LCP) were utilized as the initial states of two independent MD simulations of the NCS-1 protein.[26] This is in line with our aim to investigate in atomistic detail how the elevated temperature influences the interaction between the HC pocket and loop L3 in the absence of PEG molecules. The two initial states were labeled as iWT-1, iWT-2. The backbone root mean square deviations (RMSDs) of the residues E11 to K174 of the human NCS-1 protein were 0.18 nm for iWT-1—iWT-2 pair.

MD Simulation Protocols.

MD simulations have been widely used in the conformational studies of biomolecules.[32–38] In this study, MD simulations were carried out using the GROMACS 4.5.3 software package[39] and the CHARMM27 force field with CMAP corrections,[40] in accordance with the recent MD studies by Bellucci et al.[25] and by us.[27, 41] The results from these two MD studies were consistent with a recent experimental study.[26] The force-fields used in this work are reliable with the four force fields including CHARMM27 providing a reasonably accurate description of the native states of two small proteins with -helix and -sheet structures,[42] close to the ensembles that were reconstructed to fit the experimental data.[43] Two independent 500 ns MD simulations were performed respectively at 310 K and at 316 K, using model-1 and model-2 with the three calcium ions in the PDB structure (PDB id: 2LCP)[26] as starting points. In this study, the parameters used for the calcium ions were: q = +2.0 e, σ = 0.2436 nm and ε = 0.5021 kJ/mol. To inspect the structure of the Ca^{2+} binding sites of the NCS-1 protein, we plotted in Figure S1 the average distances between the three Ca^{2+} ions and the coordinating atoms around of them during the time scale of 0~500 ns. The average distances fluctuated around 0.2–0.3 nm during the full 500 ns simulation time, indicative of the structural stability of the Ca^{2+} ions binding sites, consistent with our results.[41] The simulation box type was rhombic dodecahedron and the edge length of the boxes respectively 9.30 × 9.30 × 6.58 × 4.65 × 4.65 nm for iWT-1 and 9.16 × 9.16 × 6.47 × 4.58 × 4.58 nm for iWT-2 systems. The boxes were big enough that the contact probability between the protein and its own periodic image in each MD simulation was less than 0.04%. The TIP3P water model was used. Additional NaCl was added to the system with a concentration of 0.1 M. Bond lengths with hydrogen atoms were constrained by the LINCS[44] and SETTLE algorithms,[45] allowing an integration time step of 2 fs. Particle mesh Ewald (PME) method was used to calculate the electrostatic interaction with a real space cutoff of 1.0 nm, and the van der Waals interactions were calculated using a cutoff of 1.4 nm. The simulations were performed in isothermal-isobaric (NPT) ensemble using periodic boundary conditions. The solute and solvent were separately coupled to external temperature bath using velocity rescaling method[46] and pressure bath using the Parrinello-Rahman method.[47] The temperature and pressure were maintained at 310 K, 316 K and 1 bar using coupling constants of 0.1 and 1.0 ps, respectively.

Analysis Methods.

Analysis of the trajectory was performed using the tools implemented in the GROMACS 4.5.3 software package.[39] The RMSDs were calculated following structural alignment. The backbone RMSDs of the core structure (residues E11-K174), the N-domain (residues E11-S93) and the C-domain (residues D98-K174) of NCS-1 protein were respectively calculated. The structural stability of the NCS-1 protein was further examined by the time evolution of the number of backbone H-bonds. A hydrogen bond was considered to be formed if the distance between N and O is ≤ 3.5 Å and the angle of N-H…O is ≥150°. The DSSP program was used to determine the secondary structure.[48] Root mean square fluctuation (RMSF) was calculated for each residue with respect to the MD generated average structure during the time scale of 200–500 ns. The potential mean force (PMF or free energy landscape) was constructed using the relation -RT ln H(x, y), where H(x, y) was the histogram of two selected reaction coordinates, x and y. The graphical structure analysis was performed using

the tools implemented in the visual molecular dynamics (VMD 1.9.1) package.[49] The optimal and suboptimal paths and the dynamical communities networks of the NCS-1 protein were analyzed and displayed by Network View[50] implemented in VMD. A salt bridge between a pair of oppositely charged residues was considered to be formed if the centroids of the side-chain charged groups in oppositely charged residues lay within 0.4 nm of each other.[51] The distances between the centroids of the side-chain charged groups were calculated to obtain the change of the salt bridges.

3. RESULTS AND DISCUSSION

Human NCS-1 protein maintained the overall secondary structure content at elevated temperature.

The NMR solution structure of unmyristoylated calcium-bound human NCS-1 protein has been solved.[26] A cartoon representation of the NCS-1 protein with three Ca^{2+} ions is given in Figure 1a. The structure is characterized by four helix-loop-helix EF-hand motifs (blue arrows). The four EF-hands, EF1, EF2, EF3 and EF4, occur in EF domain pairs.[52] The N-domain (residues M1-S93) consists of EF1 and EF2, and the C-domain (residues D98-V190) consists of EF3 and EF4.[26] The two pairs are connected via a hinge loop (residues R94-L97). Three of the four EF hands (EF2, EF3, and EF4) bind Ca^{2+} ions. According to Heidarsson et al.,[26] the nine α-helices are helix 1 (H1) (residues E11~R18), H2 (E24~F34), H3 (A45~Q54), H4 (T62~F72), H5 (F82~S93), H6 (D98~Y108), H7 (R118~V132), H8 (E146~M155), H9 (L166~K174). Helices H2 to H9 shape a hydrophobic crevice (HC), of which helices H4, H5, and H6 form the floor of the crevice, H3 and H7 on one side and H9 on the other side, helices H2 and H8 close the HC at the opposite edges. The three loops are L1 (F56~P61) connected helices H3 and H4, L2 (G133~P145) between helices H7 and H8, and L3 (D176~V190) located in the C-terminal tail of the protein.

We first examined the conformational dynamics of NCS-1 protein at 310 K by performing two independent 500 ns MD simulations in NPT. To make direct comparison, the backbone RMSDs of the core structure (residues E11-K174), N-domain (residues E11-S93) and C-domain (residues D98-K174) of NCS-1 at two different temperatures are calculated. Figure 1 presents the time evolution of the backbone RMSDs of the core structure, N-domain and C-domain of NCS-1 with respect to the corresponding energy minimized initial state in the two different MD trajectories. The backbone RMSDs of the core structure (black curve in b, e) at 310 K increase quickly within the first 50 ns, then change gradually and stabilize respectively around 0.32 and 0.43 nm after t=150 ns for both systems, indicating that the NCS-1 protein maintained its native structure within the time scale of 0~500 ns at 310 K. The backbone RMSDs of the N-domain show a similar tendency with those of the core structure and stabilize respectively around 0.29 and 0.40 nm for WT1 and WT2 during the last 400 ns. While the RMSD values of the C-domain change gradually and finally maintain respectively around 0.32 and 0.35 nm during the time scale of 100~500 ns and 320~500 ns.

The structural stabilities of the NCS-1 protein at 316 K were then probed using two independent MD runs initiated from two different energy-minimized initial conformations (iWT-1, iWT-2) as those at 310 K. As shown in Figure 1, the backbone RMSDs of the protein at 316 K in Figure 1 (red curve) overlapp well with those at 310 K, revealing similar

overall conformational dynamics of NCS-1 protein at the different temperatures. The RMSD values of the C-domain in WT2 at 316 K are larger than those of at 310 K during the time of 50~300 ns. To examine what happens in the C-domain for WT2 during the MD simulations time scale, we monitor the number of backbone H-bonds and the percentage of helix as a function of time in Figure S2. The number of backbone H-bonds (a, b) fluctuates around 80 and the helix percentage (c, d) remains around 55% during the MD simulations at 310 K (black curve), indicating that the native structure of NCS-1 is dynamically stable and remains mostly unchanged in aqueous solution, consistent with a recent MD study by Bellucci et al.[25] and us[27, 41]. The curves of the number of backbone H-bonds at 316 K for the NCS-1 protein in Figure S2 (red curve (a), (b)) overlapp well with those at 310 K, revealing similar global conformational dynamics. The curves of the percentage of helix at 316 K (red curve (c), (d)) fluctuate respectively around 55% and 50% during the 500-ns duration of MD simulations. The percentage of helix of WT2 NCS-1 protein is a bit less at 316 K than that at 310 K. The fluctuation in the number of H-bonds corresponds to disruption and reformation of backbone H-bonds and those of the helix percentage show the partial unfolding-refolding of helices. To obtain a clearer picture, the secondary structure profile was calculated as a function of time and shown in Figure S3. Figure S3d illustrates that the partial unfolding-refolding event in the C-domain involves mostly helix H8 (residues E146~M155) and loop L3 (residues D176~V190). Helix H8 partially unfolds and changes into turn (in yellow) or bend (in green) during the time period of 25~250 ns, and refolds into helix after t=250 ns. The α-helix in loop L3 keeps unfolding-refolding during the whole MD simulation at 310 K, while it vanishes at 316 K. The larger RMSD value of the C-domain in Figure 1g indicates that the tertiary structure may undergo certain conformational rearrangements with time while the secondary structure and the overall folding of NCS-1 protein remain mostly unchanged.

The partial unfolding-refolding of the helices is accompanied by the breaking and reformation of the backbone hydrogen bonds which are prerequisite of helix formation. The reduction of the helix percentage of WT2 NCS-1 at 316 K is also seen clearly in the probability of the H-bonds number in Figure S4. The average numbers of H-bonds in the two MD trajectories at 310 K are also 82, while those are respectively 82 and 79 at 316 K. These data, especially in WT2, indicate that with the elevated temperature the protein is slightly less stable yet maintain the global secondary structure.

After examining the global structural changes of NCS-1 protein at two different temperatures, we further investigated local conformational dynamics by calculating the Cα root-mean-square fluctuation (RMSF) relative to the MD-generated average structure in the time scale of 200~500 ns. Figure S5 shows the Cα-RMSF at 310 K and 316 K from the two independent MD runs. Except for few regions, the RMSF at 316 K (Figure S5 red curve) overlaps well with those at 310 K (black curve), revealing similar fluctuations of the NCS-1 protein at two different temperatures.

Elevation of the temperature expands the global protein structure.

Comparing the three-dimensional (3D) cartoon representations drawn for the structures obtained at the end of the MD simulation in Figure S6, we found that the size of the protein

was obviously larger at 316 K than at 310 K. Then the radius of gyration (*Rg*) for the two different systems was further calculated. The Rg of the protein at different temperatures are shown in Figure S7 and the significant difference can be seen in these two figures. The Rg at 310 K (black curve) reduces quickly from the start of MD simulation, then changes gradually and stabilizes respectively around 1.72 nm and 1.75 nm at the last 450 and 300 ns. While the Rg of protein at 316 K reduces quickly within the first 50 ns, then fluctuates and stabilizes at about 1.77 nm and 1.82 nm at the end of the simulations. The curve of WT1 fluctuates at about 1.90 nm during the time scale of 50–250 ns, then reduces gradually and finally stabilizes at about 1.77 nm. In the four MD trajectories, the Rg at 316 K is obviously larger than at 310 K, indicating that the elevated temperature induces global structural expansion. However, a well-folded structure at 316 K is still maintained as shown in Figures S3 and S6.

To further understand the structural properties of the NCS-1 protein at different temperatures, the potential of mean forces (PMF) of the protein at 310 K and 316 K were calculated in Figure 2. The potential of mean forces are projected onto two reaction coordinates: the radius of gyration and the number of H-bonds. Apart from the WT1 system at 316 K, the other three potential of mean force plots are similar and there is one global minimum-energy basin in Figure 2. One basin (in blue) is located at (Rg, number of H-bonds) value of (1.72 nm, 80) and (1.74 nm, 80) at 310 K (a, b). In contrast, two basins appearing in WT1 protein are located at (Rg, number of H-bonds) value of (1.78 nm, 80) and (1.88 nm, 78) (c), and One basin is located at (Rg, number of H-bonds) value of (1.81 nm, 78) (d) at 316 K. It can be seen that the basin is very narrow in Figure 2a corresponding to the relatively stable Rg value, while in Figure 2c there are changes to the two elliptical basins corresponding to simulation time duration respectively of 50–250 and 250–500 ns. The potential of mean force plots of the NCS-1 protein are changed and the global minimum-energy basins of PMF move to the right and down with the elevated temperature. The data demonstrate that the elevated temperature changes the free energy surface of the NCS-1 protein. Interestingly, the number of hydrogen bonds does not weaken with increasing temperature, consistent with the observation of conserved secondary structure and overall protein folding at 316 K.

Loop L3 adopts a more extended state and occupies the hydrophobic crevice to a larger extent with the elevation of temperature.

Figure S3b shows that the α-helical structure at C-terminal tail (residue D176-V190) simultaneously unfolds and refolds during the time period of t=0~500 ns at 310 K, changing among the turn (in yellow), bend (in green) and the α-helix (in blue). In contrast, the α-helix disappears at 316 K. Figure S6 shows that the short α-helix spans residues S178-L185 at 310 K while loop L3 adopts a more extended state and occupies the HC to a larger extent at 316 K. The only partially bound HC at 310 K may facilitate incoming ligand binding while the more occupied HC at 316 K could hamper L3 release thus inhibit ligand binding, which may affect the binding of the protein to its receptors.

The C_α–C_α distance between the starting and ending residues of loop L3 (D176 and V190) were calculated at the two temperatures. Figure 3 presents the probability distributions of the

residues D176-V190 distance for the 310 K and 316 K runs. The distance distribution peaks are centered respectively at 2.35 nm and 1.80 nm at 310 K, while the peaks are located at 2.68 nm (a), 1.60 and 2.10 nm (b) at 316 K. Two peaks appear in WT2 at 316 K, illustrating that loop L3 can be in a collapsed state albeit mainly in an extended state. The high probability of the collapsed state of loop L3 at 310 K indicates that HC is only partially occupied by loop L3, while the more extended state of loop L3 at 316 K indicates that HC may be more occupied by loop L3. The results are similar to the study by us[27] that NCS-1^{R102Q} mutation-associated functional deficits. Recently, Burgoyne and coworkers[11] showed that elevation of temperature resulted in a significant slowing of movement of the wild type *C. elegance*, while the NCS-1 null worms showed a small but significantly faster rate of movement. It is unclear whether the extents of exposure of the HC for *C. elegants* NCS-1 are changed with the elevated temperature and remain to be further explored.

Elevated temperature reduces the connectivity between residues D176 and V190 of the C-terminal tail loop L3.

An analysis of the pathways between the starting and ending residues of loop L3 can be used to assess the strength of communication between the two sites in the protein.[53] The one optimal, shortest path (blue) between the residues D176 and V190 called optimal path[50] is calculated and serves as the main path between the source node (D176) and the sink node (V190) (Figure 4). The alternate, slightly longer paths (suboptimal paths) (red)[50] were also determined for the protein at two different temperatures. There are 73 suboptimal paths at 310 K while only 2 at 316 K, indicative of a high connectivity between the two sites at 310 K while that is not present at 316 K. The optimal path involves helices H9, H8 and loops L2, L3 at 310 K and switches to only following the loop L3 at 316 K. Similar phenomenon is also seen in the suboptimal paths. The data illustrate that the number of suboptimal paths is largely reduced and the strength of communication between residues D176 and V190 decreases with the elevation of temperature.

Elevated temperature weakens the interdomain correlation and strengthens the intradomain coupling.

The community network based on the MD trajectories is used to analyze the conformational dynamics of the protein.[53] The differences in connectivity between residues[50, 53] can observe not only which individual residues are directly affected, but also which residues belong to one community. The structural properties at 310 K and 316 K can be seen from the dynamic community networks in Figure 5. Each residue has been assigned a node centered on its Cα atom, and the edges were defined to connect pairs of nodes related residues that interacted at least 75% of the time (within 4.5 A°) throughout the time duration of 0~500 ns simulation time. The time averaged connectivity of the nodes is used to identify the disjoint sub-network called community in the network.[54] Within the global dynamical network, there are more and stronger connections within the nodes belonging to the same community and weaker to nodes outside the community. The edge widths represent their weights, with the thickness indicating the strength of the dynamic correlation.

Though the network of NCS-1 protein is split into 9 communities at the two temperatures, it can be seen from Figure 5 that the dynamic community networks are significantly different.

The connections between the N-domain and C-domain are dense at 310 K, especially helices H5 and H6 belong to one community, indicating more and stronger connections between the N-domain and C-domain. In contrast, the intra-communities connections become denser and stronger at 316 K, mainly between helices H2 and H5. The results show that the elevation of temperature weakens inter-domain cross-talk and strengthens the intra-domain connections.

Of particular interest are the connections in the C-terminal tail loop L3 segment. At 310 K, there are more and stronger communications between loop L3 and part of helix H7 and loop L2 (blue), while the connections between loop L3 and helix H6 (green) become stronger at 316 K, consistent with the data in Figure 4. The data illustrate that one of the critical reasons for the reduction of the communication between residues D176 and V190 is the changed residue-residue connections.

At 316 K, although the interactions within some communities such as helices H1, H2 and H6 are enhanced, the coupling between different communities decreases. The data show that even though the secondary structure content at 316 K is largely maintained, the residue-residue connections and the dynamic communities are changed. The elevation of temperature especially weakens the global connections, illustrating the stronger inter-domain coupling which might be important for the global conformation of the protein.

Elevated temperature reduces dramatically the number and the probability of the salt bridge in the C-domain.

NCS-1 is a highly charged protein, containing 24 positively charged and 33 negatively charged residues on the protein surface. Whether in buried[55–56] or solvent-exposed[57–60] locations, salt-bridges play a critical role in stabilizing the proteins.[61–62] Recently a study showed that disruption of interfacial salt bridges largely disfavor the β-sheet-to-β-sheet association, highlighting the importance of salt bridges in the formation of cross-seeding assemblies.[63] To probe whether the elevated temperature affects the salt bridges in the N- and C-terminal domains, the probabilities of salt bridge between all positively and negatively charged residues in protein are calculated. A salt bridge is considered to be formed if the centroids of the side-chain charged groups lie within 0.4 nm of each other.[51] The more-affected salt bridges are given in Figure 6 for the protein at 310 K (a) and at 316 K (b). With the elevation of temperature, these most affected intradomain salt bridges include K9-E11, E14-R18, E15-R18, E15-K19, K25-E26, K36-D37, D37-K50, K53-D60, D44-R79, K19-E74 in N-domain, and E99-R102, R118-D150, E140-K147, E140-R148, E140-R151, E142-K147, E142-R148, R151-D176, D161-K163, E171-K174 in C-domain. The interdomain salt bridges are also affected, such as E26-R94, K63-D123, E74-R102, E74-K106 and D98-K174. Among these affected salt bridges, E15-R18, E15-K19, D44-R79, E26-R94, E99-R102, R118-D150, E142-R151 and K63-D123 were also reported in the recent MD studies by Bellucci et al.[25] and by us[27, 41], indicative that these salt bridges played critical roles in the conformational properties of the human protein.

It can be seen from Figure 6 that the salt-bridge probability maps are significantly different at 310 K and 316 K. When the temperature elevates, some salt bridges disappear, such as E14-R18, K19-E74, K25-E26, D98-K174, E140-K147, E140-R151, while K53-D60, E142-K147 are newly formed, revealing that the elevated temperature reduces dramatically the

salt-bridge number of the N-domain and C-domain. The salt-bridge probability in the C-domain obviously decreases at 316 K, including E99-R102 in H6, R118-D150 between H7 and H8, salt bridges E140-R151, E142-R148 connecting helix H8 and loop L2, E171-K174 in H9. However, the intradomain weakened interactions could be partly compensated by the interdomain salt bridges E74-R102, E74-K106 and K63-D123, maintaining a well-folded structure.

Of particular interest is the salt bridge R151-D176 related to the C-terminal tail of loop L3. With the elevation of temperature, the probability of the salt bridge R151-D176 decreases and weakens the interaction between helix H8 and the N-terminal residue D176 of loop L3, which would facilitate an unrestricted loop L3 conformation. The data illustrate that the elevated temperature could affect the mobility of loop L3, providing an explanation for loop L3 adopting a more extended state and occupying the hydrophobic crevice to a larger extent (see Figure 5).

4. CONCLUSIONS

We explored the influence of elevated temperature on the structural properties of human NCS-1 protein. Our multiple extensive MD simulations demonstrate that the protein maintains the overall secondary structure content at the elevated temperature, but the global protein structure is significantly expanded and the free energy surface of the NCS-1 protein changes. Loop L3 preferentially adopts a collapsed sate at 310 K, while it tends to have a relatively extended state at 316 K, helping loop L3 to occupy the hydrophobic crevice to a larger extent, which may hinder the binding of partners to the HC. Analysis of the communication pathways between the starting and ending residues of loop L3 shows that the elevation of the temperature alters the optimal path and largely decreases the number of suboptimal paths, indicating a reduced connectivity between residues D176 and V190 of the C-terminal tail L3. The dynamic community network analysis shows that the elevated temperature weakens the interdomain correlation but strengthened the intradomain coupling. Importantly, analysis of the salt bridge population demonstrates that the elevated temperature alters the salt bridge network, especially the salt bridges in the C-domain, which may alter the conformational dynamics of the protein.

It is interesting to compare the results from current study with previous works on the R102Q mutant and Δ176–190 truncated NCS-1.[27, 41] The R102Q mutation reduces the structural flexibility of the NCS-1 and thus disabled its function. The elevation of the temperature has similar effects as the Δ176–190 C-terminal truncation increasing structural dynamics, expansion of Rg, and changing the residue network communications. However, unlike the Δ176–190 C-terminal truncation which may reduce some hydrogen bonding network, the elevation of temperature maintains better the structural integrity of NCS-1. These structural and dynamic differences among the elevation of temperature, dysfunctional mutation, and C-terminal truncation are consistent with experimental observations of NCS-1's modulation of locomotion in *C. elegans.*[11] Therefore, we conclude that the structural and dynamics response of NCS-1 protein to elevation of temperature is likely to be one of its intrinsic functional properties.

Supplementary Material

Refer to Web version on PubMed Central for supplementary material.

ACKNOWLEDGEMENTS

We thank Dr. Ruxi Qi and Chendi Zhan for helpful discussion. This project has been funded from Graduate Student Education Innovation Plan of Shanghai University of Sports (Grant No. yjscx2015003). Simulations were performed at the High Performance Computing Server (PowerEdge T710) of Shanghai University of Sport. This project has been funded in whole or in part with Federal funds from the National Cancer Institute, National Institutes of Health, under contract number HHSN261200800001E. This research was supported (in part) by the Intramural Research Program of the NIH, National Cancer Institute, Center for Cancer Research. The funders had no role in study design, data collection and analysis, decision to publish, or preparation of the manuscript.

REFERENCES

(1). Laupland KB Fever in the critically ill medical patient. Crit. Care Med 2009, 37, S273–s278. [PubMed: 19535958]

(2). Axelrod YK; Diringer MN Temperature management in acute neurologic disorders. Neurologic clinics 2008, 26, 585–603. [PubMed: 18514828]

(3). Cremer OL; Kalkman CJ Cerebral pathophysiology and clinical neurology of hyperthermia in humans. Prog. Brain Res 2007, 162, 153–169. [PubMed: 17645919]

(4). Kimata T; Sasakura H; Ohnishi N; Nishio N; Mori I Thermotaxis of C. elegans as a model for temperature perception, neural information processing and neural plasticity. Worm 2012, 1, 31–41. [PubMed: 24058821]

(5). Wang D; O'Halloran D; Goodman MB GCY-8, PDE-2, and NCS-1 are critical elements of the cGMP-dependent thermotransduction cascade in the AFD neurons responsible for C. elegans thermotaxis. J. Gen. Physiol 2013, 142, 437–449. [PubMed: 24081984]

(6). Gomez M; De Castro E; Guarin E; Sasakura H; Kuhara A; Mori I; Bartfai T; Bargmann CI; Nef P Ca^{2+} signaling via the neuronal calcium sensor-1 regulates associative learning and memory in C. elegans. Neuron 2001, 30, 241–248. [PubMed: 11343658]

(7). Ye HY; Ye BP; Wang DY Evaluation of the long-term memory for thermosensation regulated by neuronal calcium sensor-1 in Caenorhabditis elegans. Neuroscience bulletin 2008, 24, 1–6. [PubMed: 18273069]

(8). Weiss JL; Hui H; Burgoyne RD Neuronal calcium sensor-1 regulation of calcium channels, secretion, and neuronal outgrowth. Cell. Mol. Neurobiol 2010, 30, 1283–1292. [PubMed: 21104311]

(9). Reyes-Bermudez A; Miller DJ; Sprungala S The neuronal calcium sensor protein acrocalcin: a potential target of calmodulin regulation during development in the coral acropora millepora. PloS one 2012, 7, e51689. [PubMed: 23284743]

(10). Ames JB; Lim S; Ikura M Molecular structure and target recognition of neuronal calcium sensor proteins. Front. Mol. Neurosci 2012, 5, 1–12. [PubMed: 22319467]

(11). Martin VM; Johnson JR; Haynes LP; Barclay JW; Burgoyne RD Identification of key structural elements for neuronal calcium sensor-1 function in the regulation of the temperature-dependency of locomotion in C. elegans. Mol. Brain 2013, 6, 39. [PubMed: 23981466]

(12). O'Callaghan DW; Ivings L; Weiss JL; Ashby MC; Tepikin AV; Burgoyne RD Differential use of myristoyl groups on neuronal calcium sensor proteins as a determinant of spatio-temporal aspects of Ca^{2+} signal transduction. J. Biol. Chem 2002, 277, 14227–14237. [PubMed: 11836243]

(13). O'Callaghan DW; Tepikin AV; Burgoyne RD Dynamics and calcium sensitivity of the Ca^{2+}/myristoyl switch protein hippocalcin in living cells. The Journal of cell biology 2003, 163, 715–721. [PubMed: 14638856]

(14). Burgoyne RD Neuronal calcium sensor proteins: generating diversity in neuronal Ca2+ signalling. Nat. Rev. Neurosci 2007, 8, 182–193. [PubMed: 17311005]

(15). Burgoyne RD; Haynes LP Understanding the physiological roles of the neuronal calcium sensor proteins. Mol. Brain 2012, 5, 2. [PubMed: 22269068]

(16). Heidarsson PO; Naqvi MM; Otazo MR; Mossa A; Kragelund BB; Cecconi C Direct single-molecule observation of calcium-dependent misfolding in human neuronal calcium sensor-1. Proc. Natl. Acad. Sci. U. S. A 2014, 111, 13069–13074. [PubMed: 25157171]

(17). Hendricks KB; Wang BQ; Schnieders EA; Thorner J Yeast homologue of neuronal frequenin is a regulator of phosphatidylinositol-4-OH kinase. Nat. Cell Biol 1999, 1, 234–241. [PubMed: 10559922]

(18). Handley MT; Lian LY; Haynes LP; Burgoyne RD Structural and functional deficits in a neuronal calcium sensor-1 mutant identified in a case of autistic spectrum disorder. PloS one 2010, 5, e10534. [PubMed: 20479890]

(19). Jo J; Heon S; Kim MJ; Son GH; Park Y; Henley JM; Weiss JL; Sheng M; Collingridge GL; Cho K Metabotropic glutamate receptor-mediated LTD involves two interacting Ca(2+) sensors, NCS-1 and PICK1. Neuron 2008, 60, 1095–1111. [PubMed: 19109914]

(20). Saab BJ; Georgiou J; Nath A; Lee FJ; Wang M; Michalon A; Liu F; Mansuy IM; Roder JC NCS-1 in the dentate gyrus promotes exploration, synaptic plasticity, and rapid acquisition of spatial memory. Neuron 2009, 63, 643–656. [PubMed: 19755107]

(21). Romero-Pozuelo J; Dason JS; Atwood HL; Ferrus A Chronic and acute alterations in the functional levels of Frequenins 1 and 2 reveal their roles in synaptic transmission and axon terminal morphology. Eur. J. Neurosci 2007, 26, 2428–2443. [PubMed: 17970740]

(22). Dason JS; Romero-Pozuelo J; Marin L; Iyengar BG; Klose MK; Ferrus A; Atwood HL Frequenin/NCS-1 and the Ca^{2+}-channel alpha1-subunit co-regulate synaptic transmission and nerve-terminal growth. J. Cell Sci 2009, 122, 4109–4121. [PubMed: 19861494]

(23). Braunewell KH The darker side of Ca2+ signaling by neuronal Ca^{2+}-sensor proteins: from Alzheimer's disease to cancer. Trends Pharmacol. Sci 2005, 26, 345–351. [PubMed: 15982480]

(24). Piton A; Michaud JL; Peng H; Aradhya S; Gauthier J; Mottron L; Champagne N; Lafreniere RG; Hamdan FF; Joober R; Fombonne E; Marineau C; Cossette P; Dube MP; Haghighi P; Drapeau P; Barker PA; Carbonetto S; Rouleau GA Mutations in the calcium-related gene IL1RAPL1 are associated with autism. Hum. Mol. Genet 2008, 17, 3965–3974. [PubMed: 18801879]

(25). Bellucci L; Stefano C; Felice RD; Paci E The structure of neuronal calcium sensor-1 in solution revealed by molecular dynamics simulations. PLoS One 2013, 8, e74383. [PubMed: 24098643]

(26). Heidarsson PO; Bjerrum-Bohr IJ; Jensen GA; Pongs O; Finn BE; Poulsen FM; Kragelund BB The C-terminal tail of human neuronal calcium sensor 1 regulates the conformational stability of the Ca 2+- activated state. J. Mol. Biol 2012, 417, 51–64. [PubMed: 22227393]

(27). Zhu YZ; Wu Y; Luo Y; Zou Y; Ma BY; Zhang QW R102Q mutation shifts the salt-bridge network and reduces the structural flexibility of human neuronal calcium sensor-1 protein. J. Phys. Chem. B 2014, 118, 13112–13122. [PubMed: 25343687]

(28). Ames JB; Hendricks KB; Strahl T; Huttner IG; Hamasaki N; Thorner J Structure and calcium-binding properties of Frq1, a novel calcium sensor in the yeast Saccharomyces cerevisiae. Biochemistry 2000, 39, 12149–12161. [PubMed: 11015193]

(29). Lim S; Strahl T; Thorner J; Ames JB Structure of a Ca^{2+}-myristoyl switch protein that controls activation of a phosphatidylinositol 4-kinase in fission yeast. J. Biol. Chem 2011, 286, 12565–12577. [PubMed: 21288895]

(30). Strahl T; Huttner IG; Lusin JD; Osawa M; King D; Thorner J; Ames JB Structural insights into activation of phosphatidylinositol 4-kinase (Pik1) by yeast frequenin (Frq1). J. Biol. Chem 2007, 282, 30949–30959. [PubMed: 17720810]

(31). Bourne Y; Dannenberg J; Pollmann V; Marchot P; Pongs O Immunocytochemical localization and crystal structure of human frequenin (neuronal calcium sensor 1). J. Biol. Chem 2001, 276, 11949–11955. [PubMed: 11092894]

(32). Liu P; Huang XH; Zhou RH; Berne BJ Observation of a dewetting transition in the collapse of the melittin tetramer. Nature 2005, 437, 159–162. [PubMed: 16136146]

(33). Zhou RH; Huang XH; Margulis CJ; Berne BJ Hydrophobic collapse in multidomain protein folding. Science 2004, 305, 1605–1609. [PubMed: 15361621]

(34). Garcia AE; Paschek D Simulation of the pressure and temperature folding/unfolding equilibrium of a small RNA hairpin. J. Am. Chem. Soc 2008, 130, 815–817. [PubMed: 18154332]

(35). Miyashita N; Straub JE; Thirumalai D Structures of beta-amyloid peptide 1–40, 1–42, and 1–55-the 672–726 fragment of APP-in a membrane environment with implications for interactions with gamma-secretase. J. Am. Chem. Soc 2009, 131, 17843–17852. [PubMed: 19995075]

(36). Gao YQ; Yang W; Karplus M A structure-based model for the synthesis and hydrolysis of ATP by F1-ATPase. Cell 2005, 123, 195–205. [PubMed: 16239139]

(37). Krone MG; Hua L; Soto P; Zhou RH; Berne BJ; Shea JE Role of water in mediating the assembly of Alzheimer amyloid-beta Abeta16–22 protofilaments. J. Am. Chem. Soc 2008, 130, 11066–11072. [PubMed: 18661994]

(38). Zuo GH; Huang Q; Wei GH; Zhou RH; Fang HP Plugging into proteins: poisoning protein function by a hydrophobic nanoparticle. ACS nano 2010, 4, 7508–7514. [PubMed: 21080666]

(39). Hess B; Kutzner C; van der Spoel D; Lindahl E GROMACS 4: Algorithms for highly efficient, load-balanced, and scalable molecular simulation. J. Chem. Theory Comput. 2008, 4, 435–447. [PubMed: 26620784]

(40). Bjelkmar P; Larsson P; Cuendet MA; Hess B; Lindahl E Implementation of the CHARMM force field in GROMACS: analysis of protein stability effects from correction maps, virtual interaction sites, and water models. J. Chem. Theory Comput 2010, 6, 459–466. [PubMed: 26617301]

(41). Zhu YZ; Yang S; Qi RX; Zou Y; Ma BY; Nussinov R; Zhang QW Effects of the C-terminal tail on the conformational dynamics of human neuronal calcium sensor-1 protein. J. Phys. Chem. B 2015, 119, 14236–14244. [PubMed: 26447771]

(42). Lindorff-Larsen K; Maragakis P; Piana S; Eastwood MP; Dror RO; Shaw DE Systematic validation of protein force fields against experimental data. PloS one 2012, 7, e32131. [PubMed: 22384157]

(43). Lange OF; Lakomek NA; Fares C; Schroder GF; Walter KF; Becker S; Meiler J; Grubmuller H; Griesinger C; de Groot BL Recognition dynamics up to microseconds revealed from an RDC-derived ubiquitin ensemble in solution. Science 2008, 320, 1471–1475. [PubMed: 18556554]

(44). Hess B; Bekker H; Berendsen HJC; Fraaije JGEM LINCS: A linear constraint solver for molecular simulations. J. Comput. Chem 1997, 18, 1463–1472.

(45). Miyamoto S; Kollman PA Settle- an analytical version of the shake and rattle algorithm for rigid water models. J. Comput. Chem 1992, 13, 952–962.

(46). Bussi G; Donadio D; Parrinello M Canonical sampling through velocity rescaling. J. Chem. Phys 2007, 126, 014101. [PubMed: 17212484]

(47). Parrinello M; Rahman A Polymotphic transitions in single crystals: A new molecular dynamics method. J. Appl. Phys 1981, 52, 7182–7190.

(48). Kabsch W; Sander C Dictionary of potein secondary structure: Pattern recognition of hydrogen - bonded and geometrical features. Biopolymers 1983, 22, 2577–2637. [PubMed: 6667333]

(49). Humphrey W; Dalke A; Schulten K VMD: visual molecular dynamics. J. Mol. Graphics 1996, 14, 33–38, 27–28.

(50). Eargle J; Luthey-Schulten Z NetworkView: 3D display and analysis of protein.RNA interaction networks. Bioinformatics 2012, 28, 3000–3001. [PubMed: 22982572]

(51). Ma BY; Kumar S; Tsai CJ; Nussinov R Folding funnels and binding mechanisms. Protein Eng., Des. Sel 1999, 12, 713–720.

(52). Gifford JL; Walsh MP; Vogel HJ Structures and metal-ion-binding properties of the Ca2+-binding helix-loop-helix EF-hand motifs. Biochem. J 2007, 405, 199–221. [PubMed: 17590154]

(53). Sethi A; Eargle J; Black AA; Luthey-Schulten Z Dynamical networks in tRNA:protein complexes. Proc. Natl. Acad. Sci. U. S. A 2009, 106, 6620–6625. [PubMed: 19351898]

(54). Girvan M; Newman ME Community structure in social and biological networks. Proc. Natl. Acad. Sci. U. S. A 2002, 99, 7821–7826. [PubMed: 12060727]

(55). Waldburger CD, Schildbach JF, Sauer RT Are buried salt bridges important for protein stability and conformational specificity? Nat. Struct. Mol. Biol 1995, 2, 122–128.

(56). Tissot AC; Vuilleumier S; Fersht AR Importance of two buried salt bridges in the stability and folding pathway of barnase. Biochemistry 1996, 35, 6786–6794. [PubMed: 8639630]

(57). Makhatadze GI; Loladze VV; Ermolenko DN; Chen X; Thomas ST Contribution of surface salt bridges to protein stability: guidelines for protein engineering. J. Mol. Biol 2003, 327, 1135–1148. [PubMed: 12662936]

(58). Ibarra-Molero B; Zitzewitz JA; Matthews CR Salt-bridges can stabilize but do not accelerate the folding of the homodimeric coiled-coil peptide GCN4-p1. J. Mol. Biol 2004, 336, 989–996. [PubMed: 15037063]

(59). Williams DV; Byrne A; Stewart J; Andersen NH Optimal salt bridge for Trp-cage stabilization. Biochemistry 2011, 50, 1143–1152. [PubMed: 21222485]

(60). Andersson HS; Figueredo SM; Haugaard-Kedstrom LM; Bengtsson E; Daly NL; Qu X; Craik DJ; Ouellette AJ; Rosengren KJ The alpha-defensin salt-bridge induces backbone stability to facilitate folding and confer proteolytic resistance. Amino acids 2012, 43, 1471–1483. [PubMed: 22286872]

(61). Kumar S; Tsai CJ; Ma BY; Nussinov R Contribution of salt bridges toward protein thermostability. J. Biomol. Struct. Dyn 2000, 17, 79–85. [PubMed: 22607409]

(62). Kumar S; Ma BY; Tsai CJ; Nussinov R Electrostatic strengths of salt bridges in thermophilic and mesophilic glutamate dehydrogenase monomers. Proteins 2000, 38, 368–383. [PubMed: 10707024]

(63). Zhang M; Hu R; Chen H; Chang Y; Ma J; Liang G; Mi J; Wang Y; Zheng J Polymorphic cross-seeding amyloid assemblies of amyloid-beta and human islet amyloid polypeptide. Phys. Chem. Chem. Phys 2015, 17, 23245–23256. [PubMed: 26283068]

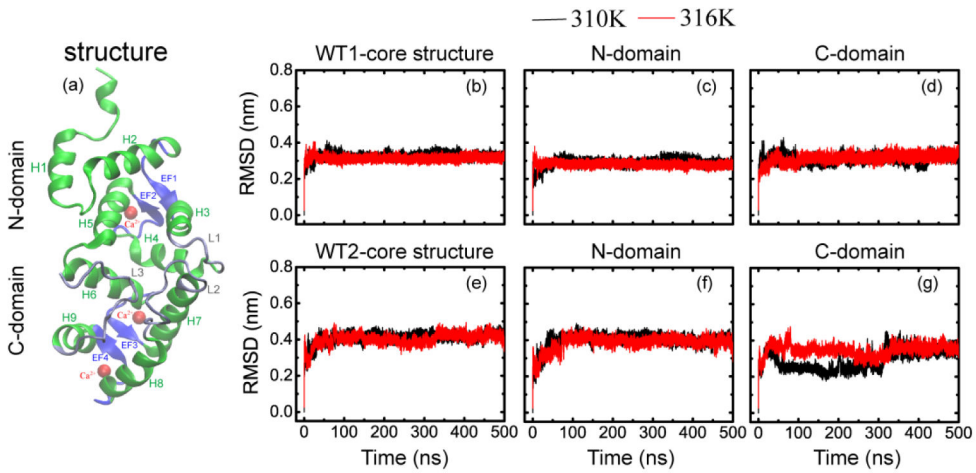

Figure 1.

(a) Cartoon diagram of the NMR structure of unmyristoylated calcium-bound human NCS-1 (PDB: 2LCP, model 1). For each segment, we use the same color in the structure as in the amino acid sequence. Blue arrows: beta sheets forming the EF-hand motifs, red balls: Ca^{2+} ions. (b~g) time evolution of the backbone RMSD values for NCS-1 protein at 310 K (black curve) and at 316 K (red curve) in two different MD trajectories (WT1, WT2). The backbone RMSDs include the core structure (E11~K174), N-domain (residues E11-S93) and C-domain (residues D98-K174) with respect to the corresponding energy-minimized initial structures (iWT-1, iWT-2) of NCS-1 (aligned on all backbone atoms from residues E11~K174, E11-S93 and D98-K174).

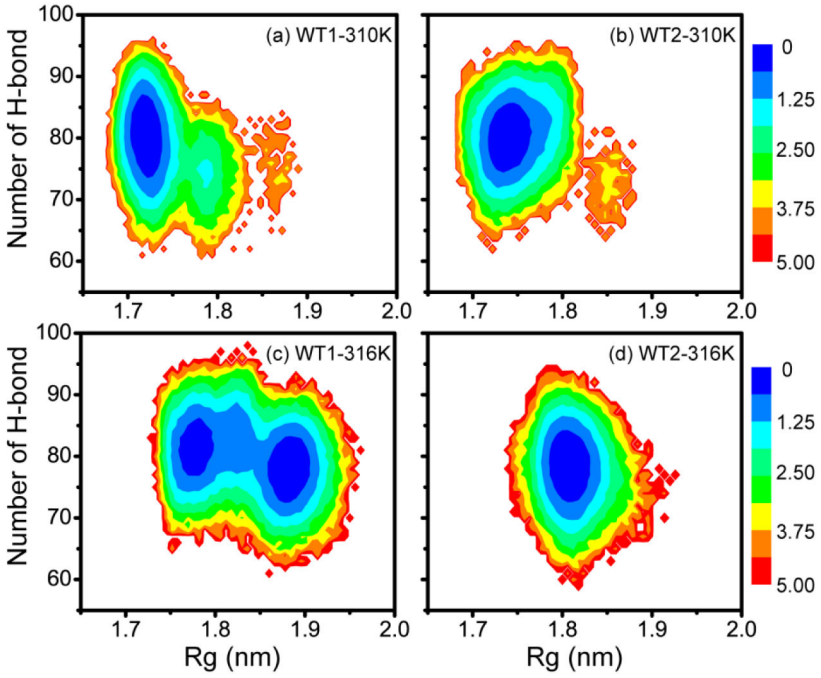

Figure 2.

Potential of mean force for NCS-1 protein at 310 K (a, b) and at 316 K (c, d), plotted as a function of the radius of gyration (Rg) and the number of H-bonds during the time scale of 0–500 ns. The unit of potential of mean force is kcal/mol.

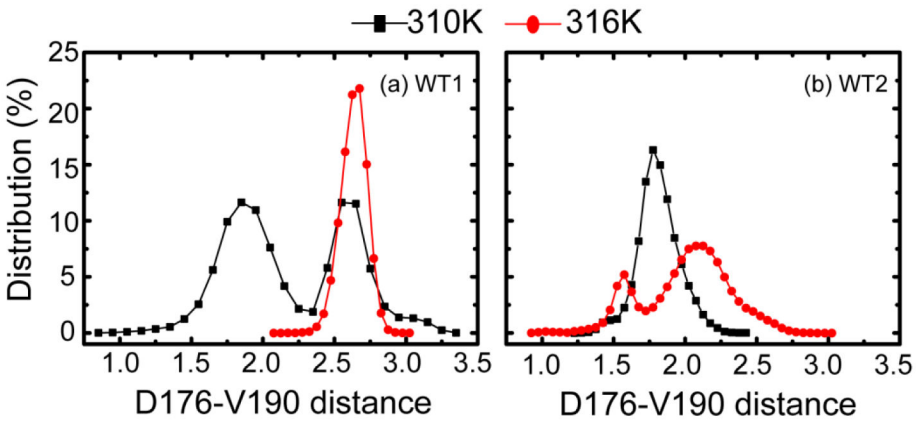

Figure 3.

Distributions of the C_α-C_α distance between the starting and ending residues of the C-terminal tail loop L3 (D176 and V190) for the NCS-1 protein respectively at 310 K (black curve) and 316 K (red curve) in two independent MD runs. The D176-V190 distances were calculated during the time scale of 200 ~500 ns of each MD trajectory for both systems.

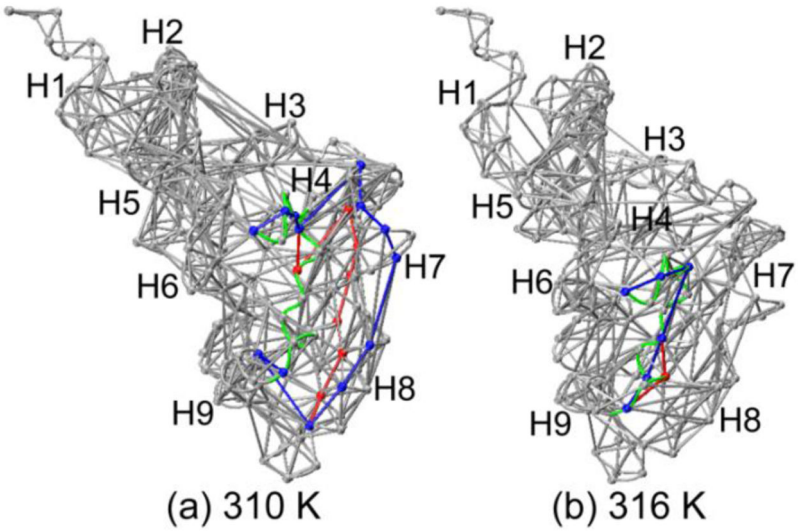

Figure 4.

Optimal and suboptimal paths connecting the residues D176 and V190 of the C-terminal tail loop L3 for (a) 310 K and for (b) 316 K. The optimal path (blue) and mainly suboptimal paths (red) were shown for the protein. Spheres indicate residue nodes in the paths. The thickness of each edge is proportional to the number of suboptimal paths that cross it during the calculation. Loop L3 segment is shown in green.

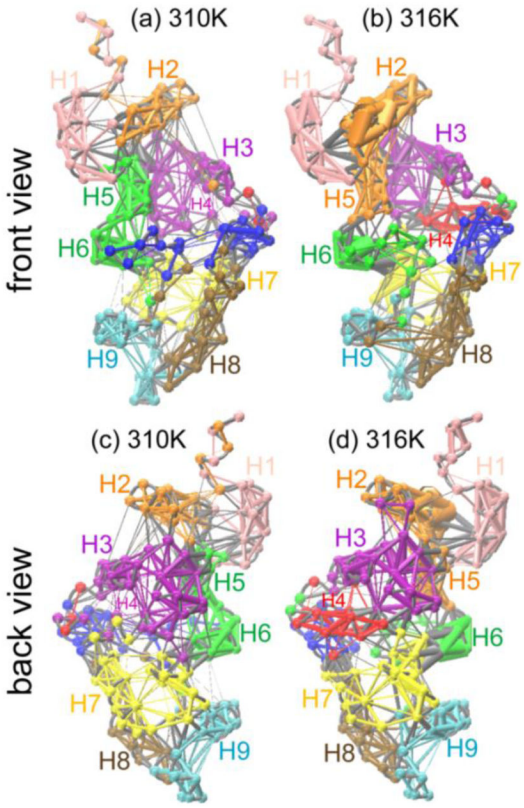

Figure 5.

Community networks formed by the representative structure of NCS-1 protein at 310 K (a) and 316 K (b) with edge widths corresponding to their weights based on MD simulations. Each community has its own color, superimposed on the respective initial MD simulation structure. The corresponding back view structures are shown in (c) and (d). The community network from the MD trajectory uses the data from 0 to 500 ns.

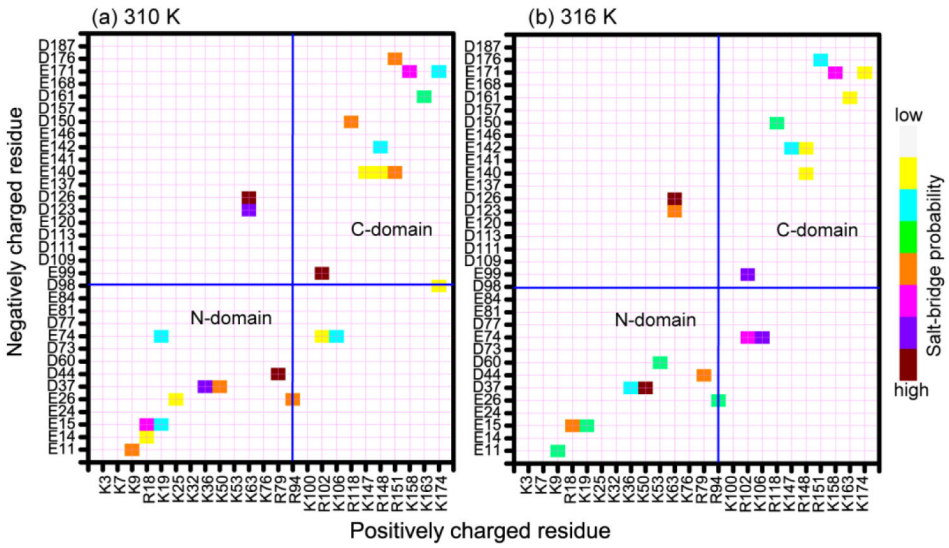

Figure 6.

Elevation of the temperature alters the salt bridge network of NCS-1 protein. The salt-bridge probability maps are given in (a) for 310 K and in (b) for 316 K of human NCS-1 protein.